HDAC Inhibition by Trichostatin A in U266 Multiple Myeloma: Anti-Proliferative Effects, Transcriptomic Dysregulation, Core Gene Clusters, and Survival-Associated Biomarkers

Ismail NH[ab], Mohamed Yusoff S[a], Husin A[c], Johan MF[a]*

[a]Department of Haematology, School of Medical Sciences, Universiti Sains Malaysia, Kelantan, Malaysia
[b]Department of Pathology, Hospital Raja Perempuan Zainab II, Kelantan, Malaysia
[c]Department of Internal Medicine, School of Medical Sciences, Universiti Sains Malaysia, Kubang Kerian, Kelantan, Malaysia

***Corresponding Author**: Assoc. Prof. Dr. Muhammad Farid Johan
Department of Haematology, School of Medical Sciences, Universiti Sains Malaysia, Kelantan, Malaysia.
Email: faridjohan@usm.my

ABSTRACT

INTRODUCTION: Histone deacetylases (HDACs) regulate chromatin and gene expression, and their dysregulation contributes to multiple myeloma (MM). This study evaluated the epigenetic effects of the HDAC inhibitor Trichostatin A (TSA) on U266 MM cells, its impact on proliferation, transcriptomic alterations, core gene clusters, and association with MM survival. **MATERIALS AND METHODS**: U266 cells were treated with TSA and assessed by MTT assays to determine IC_{50} values. Cell cycle arrest and apoptosis were measured by flow cytometry. RNA-Seq identified differentially expressed genes, followed by KEGG analysis. PPI networks and core gene clusters were generated using STRING and Cytoscape MCODE, and Kaplan-Meier plots evaluated their associations with survival outcomes. **RESULTS:** TSA induced dose-dependent cytotoxicity (IC_{50} =54.46±4.0 nM) and triggered significant G_0/G_1 arrest (82.98±1.99%), reduced S-phase (9.02±1.99%), and early and late apoptosis rates increased (24.88±2.08% and 24.86±3.81%, respectively. Transcriptomic analysis revealed enriched KEGG pathways including ECM receptor interaction ($q=2.05\times10^{-4}$), microRNAs in cancer ($q=7.52\times10^{-4}$), and cell cycle ($q=9.05\times10^{-4}$). Three core gene clusters emerged: Cluster 1 (seed gene OASL; includes *IFI44*, *RSAD2*, *IFIT3*, *MX1*, *IFIT1*, *IFI44L*, *XAF1*, *IFI6*), Cluster 2 (*NRCAM*; includes *SPTBN4*, *SPTA1*, *ANK*1), and Cluster 3 (*LRP1*; includes *APOE*, *LRP2*). *APOE* upregulation was most strongly correlated with improved survival (log rank $p<1\times10^{-16}$), with *RSAD2*, *XAF1*, *IFIT1*, and *SPTBN4* also significant ($p\leq0.05$). **CONCLUSION:** TSA exerts potent anti-proliferative effects in U266 MM cell line via several mechanisms. Survival-associated core genes Apolipoprotein E (*APOE*) and Radical S-Adenosyl Methionine Domain Containing 2 (*RSAD2*) have potential as candidate survival-associated biomarkers and therapeutic targets warrant further validation.

KEYWORDS: Multiple Myeloma, Trichostatin A (TSA), Histone Deacetylase Inhibitor (HDACi), Transcriptomic Dysregulation, Survival-Associated Biomarkers

INTRODUCTION

Multiple myeloma (MM) is a malignant disorder of terminally differentiated plasma cells that accumulate in the bone marrow and secrete abnormal monoclonal immunoglobulins.[1] These pathological changes lead to bone destruction, anaemia, renal impairment, and recurrent infections.[2] Although recent therapeutic advances such as proteasome inhibitors, immunomodulatory agents, and monoclonal antibodies have improved survival outcomes, MM remains incurable for most patients due to relapse and the emergence of drug-resistant clones.[3-5] These challenges underscore the urgent need for novel therapeutic approaches that can target molecular pathways underlying MM progression and treatment resistance.[6,7]

Epigenetic dysregulation is increasingly recognised as a key driver of myelomagenesis.[8,9] Aberrant histone acetylation patterns modify chromatin structure and alter transcriptional programs governing proliferation, haematological malignancies including MM, and immune evasion.[10-12] Histone deacetylases (HDACs), which remove acetyl groups from histone and non-histone proteins, are often overexpressed in MM [13,14] and are associated with aggressive disease and reduced survival.[15,16] Consequently, HDAC inhibitors (HDACi) have gained attention as potential epigenetic drugs capable of restoring tumour suppressor activity and re-sensitising malignant cells to cytotoxic therapies.[12, 17-18]

Trichostatin A (TSA) is a potent, reversible inhibitor of class I and II HDACs that promotes histone hyperacetylation, resulting in chromatin relaxation and reactivation of silenced genes involved in cell-cycle arrest and apoptosis.[19] Preclinical studies have demonstrated that TSA exerts antiproliferative and pro-apoptotic effects in several cancers, including haematological malignancies.[20] However, the precise molecular events and transcriptomic consequences of HDAC inhibition by TSA in MM cells remain incompletely defined. A deeper understanding of these mechanisms could uncover new therapeutic targets and survival-associated biomarkers.

High-throughput transcriptomic profiling using RNA sequencing (RNA-seq) allows comprehensive characterisation of gene expression changes induced by epigenetic drugs.[22] Integrating differential expression, pathway enrichment, and protein interaction analyses provides valuable insight into the functional networks modulated by HDAC inhibition.[22,23] Such analyses can also help identify core regulatory genes associated with treatment response and survival outcomes in MM.[24-26]

Therefore, this study aimed to investigate the anti-proliferative, pro-apoptotic, and transcriptomic effects of TSA in the U266 MM cell line. By combining cytotoxicity assays, cell-cycle and apoptosis analyses, and transcriptome-wide expression profiling, we sought to elucidate the cellular and molecular mechanisms underlying TSA's activity. Furthermore, we identified key signalling pathways, core gene clusters, and survival-associated biomarkers that may provide mechanistic insight and translational relevance for HDAC inhibition in MM.

MATERIALS AND METHODS

Cell culture

U266 cell line (ATCC, Rockville, MD, USA) were cultured in RPMI 1640 medium (Thermo Fisher Scientific, MA, USA) supplemented with 15% fetal bovine serum (Tico Europe, Netherlands) and 1% penicillin-streptomycin (Nacalai Tesque, Japan) in 95% humidified air with 5% CO^2 at 37 ºC.

3-(4,5-dimethylthiazol-2-yl)-2,5-diphenyltetrazolium bromide (MTT) assay and half maximal inhibitory concentration (IC^{50})

Cell lines were plated one day before drug treatment in 96-well plates at a density of 2×10^4 cells per well in a final volume of 90µl, with untreated cells serving as the control. After 24 hours of incubation, the cells were treated with TSA at concentrations ranging from 10nM to 150µM. Following 48 hours of incubation, an MTT assay (Nacalai, Japan) was performed according to the manufacturer's instructions. Dose-response curves were generated using GraphPad Prism Software to determine the IC^{50} values of each drug.

Cell cycle arrest and apoptosis analysis

U266 cells were seeded at a density of 1×10^6 cells per well in 6-well plates and incubated overnight. The following day, cells were treated with 300µl of the respective drugs at their IC_{50} concentrations and further incubated at 37°C for 48 h. Untreated U266 cells cultured under identical conditions served as the control samples for both cell cycle and apoptosis analyses.

Cell cycle progression was assessed using the Cycletest™ Plus DNA Reagent Kit (BD Biosciences, San Jose, CA, USA), and apoptosis was evaluated using the FITC Annexin V Apoptosis Detection Kit I (BD Biosciences, San Jose, CA, USA), according to the manufacturer's instructions. Flow cytometry analysis was performed using a BD FACSCanto™ flow cytometer (BD Biosciences), with at least 10,000 events acquired per sample.

For gating, debris and cell aggregates were excluded based on forward and side scatter properties, and doublets were eliminated using DNA area versus width parameters. Cell cycle phase distribution (G_0/G_1, S, and G_2/M) was determined from DNA content histograms using ModFit LT software version 5.0 (Verity Software House, Topsham, ME, USA). Apoptotic populations were gated based on Annexin V–FITC and propidium iodide staining to distinguish viable, early apoptotic, late apoptotic, and necrotic cells, and analysed using FCS Express 4 flow cytometry software (De Novo Software, Glendale, CA, USA).

RNA Extraction

Total RNA was extracted using the PrimeWay Total RNA Extraction Kit (Axil Scientific Pte. Ltd., Singapore). RNA concentration and purity were determined with a NanoDrop 2000 spectrophotometer (Thermo Scientific, MA, USA), ensuring a 260/280 nm absorbance ratio >1.8. RNA integrity was assessed using an Agilent 2100 Bioanalyzer (Agilent Technologies, Waldbronn, Germany). The 28S/18S rRNA ratio and 5S peak percentage were analyzed using Bioanalyzer 2100 Expert software. Samples with an RNA Integrity Number (RIN) ≥7 were selected for mRNA library preparation and sequencing.

RNA Sequencing and bioinformatics data analysis

A total of 1 µg of high-quality RNA was used for library preparation following the manufacturer's instructions for the Illumina NovaSeq 6000 System (Illumina, CA, USA). Sequencing data were processed using Bcl2fastq and Illumina's integrated software, and raw reads passing quality filters were stored in FASTQ format. Data quality was assessed using FastQC, maintaining a sequencing error rate threshold below 0.5 per base position (QPhred). Adapter trimming and quality filtering were performed with Cutadapt, and the filtered reads were aligned to the reference genome using HISAT2. Alignment files were generated in BAM format and visualized in the Integrative Genomics Viewer (IGV) to examine read distribution and transcriptional activity across chromosomes. Gene expression levels were quantified using HTSeq and expressed as Fragments Per Kilobase of transcript per Million mapped reads (FPKM).

Gene differential expression analysis

Differential gene expression analysis was performed using the DESeq2 package (v1.6.3) in Bioconductor, which models count data based on a negative binomial distribution. The analysis identified genes that were

significantly upregulated or downregulated between treatment and control groups. Genes with a fold change (FC) >2 and an adjusted p-value (q-value, FDR) <0.05 were considered significantly differentially expressed.

KEGG enrichment analysis

KEGG pathway enrichment analysis was performed using the KEGG database. Upregulated and downregulated genes were analyzed separately to identify pathways enriched in each group. Significance was determined using a hypergeometric test with Q-value ≤0.05, and the top 30 pathways were visualised as histograms and scatter plots.

Functional Protein Association Analysis

Protein–protein interaction (PPI) analysis of DEGs with $\log_2$ FC ≥2 was conducted using STRING (version 12.0). The interaction score was set to high confidence (0.900), and unconnected nodes were excluded from the network. The resulting interaction data, exported in TSV format, were imported into Cytoscape (version 3.10.1) for network visualization. Functional modules and core gene clusters were identified using the MCODE plugin.

Kaplan–Meier survival analyses of the core genes

Kaplan–Meier survival analyses of the core genes in MM were performed using the Kaplan-Meier Plotter online tool (https://kmplot.com/analysis/) on publicly available MM patient mRNA expression datasets (n=1416). Patients were stratified into high- and low-expression groups based on median gene expression to assess the association between core gene expression and overall survival. Cell lines were used only for in vitro functional assays and were not included in the survival analysis.

Statistical Analysis

Statistical analyses for IC_{50} determination, apoptosis, and cell cycle assays were performed using GraphPad Prism (version 8.0). Data are presented as mean ± standard deviation (SD) from three independent experiments. Statistical significance was assessed using two-way ANOVA followed by Tukey's post hoc test, which allows for multiple pairwise comparisons while controlling for Type I error, with $p \leq 0.05$ considered significant.

RNA-seq data quality was evaluated using RSeQC (version 2.6.3) to generate saturation curves and assess sequencing homogeneity via the geneBody_coverage.py script, which divided transcripts into 100 bins and normalized read depth. Spearman and Kendall-tau correlation analyses were applied to evaluate gene expression relationships, with R^2 >0.8 indicating a strong linear correlation. Kaplan-Meier survival analysis was used to determine the survival-associated biomarkers relevance of core genes, with significance defined at log-rank $p \leq 0.05$.

RESULTS

TSA treatment markedly inhibited the proliferation of U266 MM cells in a dose-dependent manner, with an IC_{50} of 54.46 nM after 48 hours of exposure (Figure 1(A). Cell cycle analysis showed that the population consisted of 64.68±3.10% of cells in G_0/G_1, 27.32±3.10% in S phase, and 8.00±0% in G_2/M, represented

as mean ± SD of three independent experiments. Exposure to TSA significantly arrested cells in the G_0/G_1 phase, increasing the population to 82.98±1.99% ($p \leq 0.01$), while the S-phase fraction decreased to 9.02±1.99% ($p \leq 0.01$) as shown in Figure B(ii). The G_2/M population remained unchanged, indicating that TSA selectively disrupts the G_1/S checkpoint without affecting later stages of mitosis (Figure 1(B)(i), (B)(ii) and (B)(iii). These results suggest that TSA suppresses cell proliferation primarily through early cell-cycle blockade.

Flow cytometric assessment of apoptosis and cell viability demonstrated that TSA induces extensive programmed cell death. Late and early apoptotic populations were predominant, comprising 24.88±2.08% ($p \leq 0.001$) and 24.86±3.81% ($p \leq 0.01$), respectively, indicating progressive membrane compromise. Necrotic cells increased modestly to 3.61 ± 0.10% ($p \leq 0.05$), suggesting secondary membrane damage following apoptosis rather than primary necrotic induction. Overall, TSA treatment reduced the proportion of live cells to 51.88±0.90% ($p \leq 0.01$), highlighting its dual capacity to inhibit proliferation and trigger apoptosis in MM cells (Figure 1(C)(i), (C)(ii), and (C)(iii).

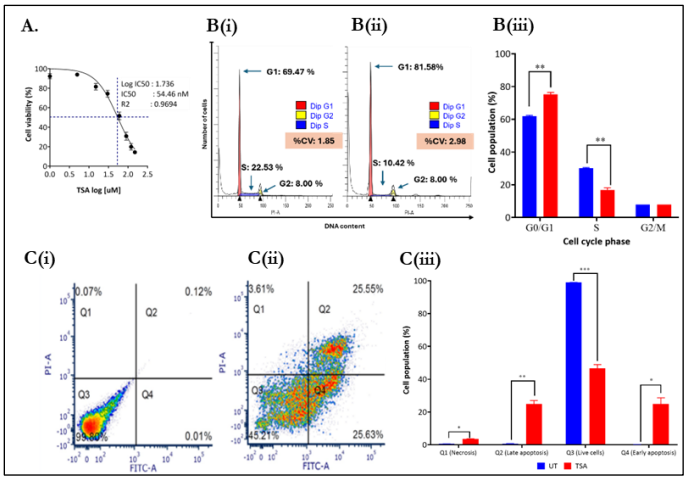

Figure 1: (A) Dose-dependent cytotoxicity of Trichostatin A (TSA) in U266 cells after 48 hours, showing cell viability and IC_{50} values. **B(i, ii)**. Representative histograms of cell cycle distribution in untreated (B(i)) and TSA-treated (B(ii)) U266 cells. TSA induces G_0/G_1 phase arrest and reduces S phase cell population. **B(iii)**. Quantification of cell cycle phases showing a significant increase in G_0/G_1 and decrease in S phase after TSA treatment (**p≤0.01). **C(i, ii)**. Flow cytometry dot plots of Annexin V-FITC/PI staining in untreated (C(i)) and TSA-treated (C(ii)) cells showing necrosis (Q1), late apoptosis (Q2), live cells (Q3), and early apoptosis (Q4). **C(iii)**. Quantification of apoptotic and necrotic cell populations showing significant increases following TSA treatment (*p≤0.05, **p≤0.01, ***p≤0.001). Data are mean ± SD from three independent experiments. Statistical analysis was performed using two-way ANOVA with Tukey's post hoc test.

Transcriptome dysregulation in TSA-treated U266 cell line

The RNA-Seq analysis revealed a total of 1,723 significant DEGs. Among these, 1187 genes were upregulated, and 536 genes were downregulated, with an FC greater than 2 and a p-value ≤0.05. Figure 2 (A) provides a volcano map illustrates outcomes of the DEG analyses, showcasing the statistical significance of the variation in gene expression between untreated and TSA-treated U266 cells. Specifically, TSA-treated U266 cells demonstrated *TMEM255B*, *PCDH1*, *ADA2*, *METTL7A*, and *SATB1*, and the most down-regulated genes were *UNC13C*, *IGFBP7*, *SPAG5*, *CCNA2*, and *MKI67* (Table S1 and Figure 2 (A)). KEGG pathway enrichment revealed that the DEGs were most significantly enriched in ECM

receptor interaction ($q=2.05\times10^{-4}$), microRNAs in cancer ($q = 7.52\times10^{-4}$), and cell cycle ($q = 9.05\times10^{-4}$) (Figure 2 (B) and Figure 2 (C)).

Table I: List of most up-and down-regulated genes in TSA treated U266.

Gene ID	Gene Symbol	Description	Log2 FC	padj	Q value
ENSG00000184497	*TMEM255B*	Transmembrane protein 255B	3.02	4.76E-90	89.32
ENSG00000156453	*PCDH1*	Protocadherin 1	4.37	7.72E-86	85.11
ENSG00000093072	*ADA2*	Adenosine deaminase 2	2.04	5.91E-64	63.23
ENSG00000185432	*METTL7A*	Methyltransferase like 7A	1.89	2.15E-58	57.67
ENSG00000182568	*SATB1*	SATB homeobox 1	1.82	3.73E-54	53.43
ENSG00000137766	*UNC13C*	Unc-13 homolog C	-1.84	2.96E-72	71.53
ENSG00000163453	*IGFBP7*	Insulin like growth factor binding protein 7	-3.31	2.53E-67	66.60
ENSG00000076382	*SPAG5*	Sperm associated antigen 5	-1.59	1.66E-65	64.78
ENSG00000145386	*CCNA2*	Cyclin A2	-1.72	3.94E-62	61.40
ENSG00000148773	*MKI67*	Marker of proliferation Ki-67	-1.75	3.46E-59	58.46

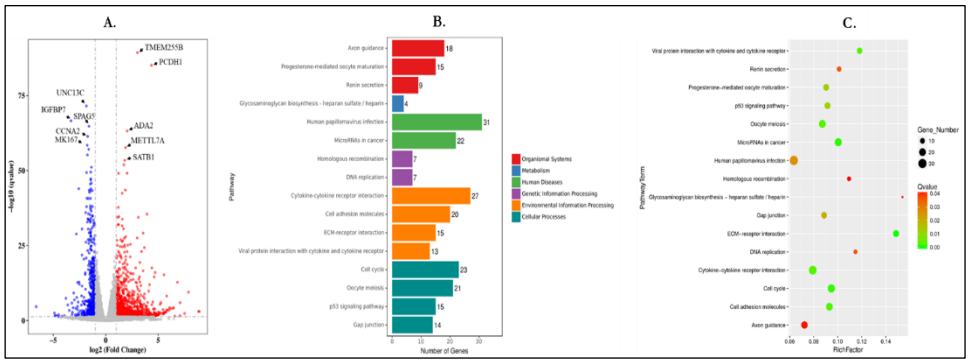

Figure 2: (A). Differential expression volcano plot, red dots represent genes that are significantly up-regulated and blue dots represent those that are significantly down-regulated in U266 cell. X axis: log2 FC of gene expression. Y axis: statistical significance of the differential expression in log10(qvalue(fdr, padj)). **(B)** KEGG pathway enrichment in TSA-treated U266 cells. The X-axis represents the number of genes mapped to each pathway, and the Y-axis indicates KEGG pathway terms. This histogram provides an overview of gene counts contributing to enriched pathways. **(C)** Scatter plot of KEGG pathway enrichment in TSA-treated U266 cells. The X-axis shows the RichFactor (ratio of DEGs to total genes in the pathway), and the Y-axis lists KEGG pathways. Point size represents the number of DEGs, and colour indicates significance (Q-value), allowing visualization of both enrichment magnitude and statistical significance.

Identification and Kaplan–Meier survival outcome of the core genes

CytoScape MCODE plugin tools illustrate the top three most significant clusters of core genes in TSA-treated U266 cell lines (Figure 3 (A). Cluster 1 displayed the highest MCODE score and featured the seed gene *OASL*, which was identified as the seed gene, with core genes including *IFI44*, *RSAD2*, *IFIT3*, *MX1*, *IFIT1*, *IFI44L*, *XAF1*, and *IFI6*. Cluster 2 was seeded by *NRCAM* and clustered with genes including *SPTBN4*, *SPTA1*, and *ANK1*. Furthermore, Cluster 3 exhibits *LRP1* as the seed gene, associated with cluster genes identified as *APOE* and *LRP2*. In TSA-treated U266 cell lines, upregulation of *APOE* (logrank P<1E-16) emerges as the most significant core gene linked with improved survival outcomes, alongside consistent outcomes in *RSAD2*, *XAF1*, *IFIT1*, and *SPTBN4* expression (Figure 3 (B)).

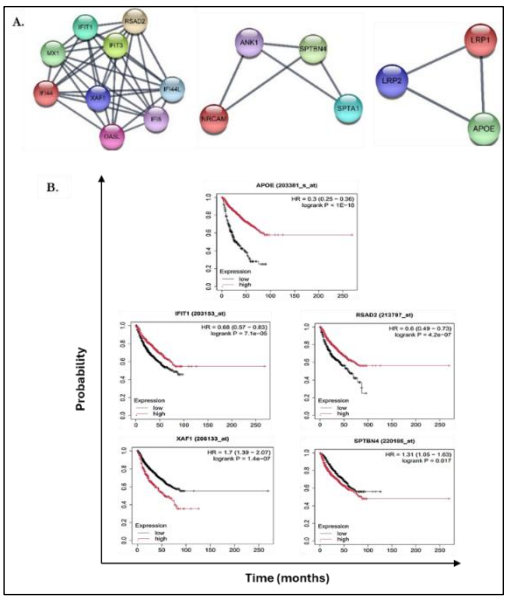

Figure 3: (A) Three main PPI network clusters of core genes identified from TSA-treated U266 cells. **(B)** Kaplan–Meier survival analyses of core genes using publicly available MM patient datasets, showing associations with overall survival (OS). Cell lines were used only for in vitro functional assays.

DISCUSSION

This study demonstrates that HDAC inhibition by TSA exerts strong anti-proliferative and pro-apoptotic effects in U266 MM cells and induces extensive transcriptomic reprogramming. The integration of cytometric and transcriptomic analyses reveals that TSA acts through a coordinated mechanism involving G_0/G_1 cell-cycle arrest, activation of apoptotic cascades, and modulation of immune-metabolic gene networks.

Cell-cycle regulation and proliferative inhibition

The observed accumulation of U266 cells in the G_0/G_1 phase, with concomitant reduction in S-phase, suggests that TSA primarily disrupts the G_1/S checkpoint. This is consistent with previous observations that HDAC inhibition induces G_1 arrest through up-regulation of CDK inhibitors (e.g., p21) and down-regulation of cyclins including cyclin A (*CCNA2*) thereby impairing DNA synthesis and mitotic progression.[27,28] In particular, TSA treatment of MM cell lines has been shown to induce G_0/G_1 arrest and lower S-phase fraction associated with decreased cyclin D1 expression.[19] The preservation of the G_2/M fraction suggests that TSA's cytostatic effect occurs before DNA replication, reflecting a targeted blockade at the early checkpoint.

Apoptotic induction and cell death mechanisms

Flow cytometry revealed that TSA treatment induced marked apoptosis in U266 MM cells, with a predominance of late apoptotic events. These observations align with previous reports showing that HDAC inhibitors promote apoptosis via activation of caspases, mitochondrial membrane depolarisation, and modulation of Bcl-2 family proteins.[29,30]

Notably, our transcriptome data indicated up-regulation of *XAF1*, which is known to antagonise the inhibitor of apoptosis protein *XIAP* and thereby facilitates intrinsic apoptotic signalling.[31] The modest increase in necrotic cells suggests that the necrosis observed is likely secondary to apoptotic membrane breakdown rather than primary necrotic induction. Collectively, these findings indicate that TSA not only halts proliferation in U266 MM cells but also actively triggers programmed cell death. Recent work in other cancer models supports the notion that HDAC inhibitors can simultaneously induce apoptosis and lead to late-stage membrane destabilisation or secondary necrosis.[32,33] For example, TSA has been shown to enhance cytotoxicity in cisplatin-treated cancer cells with increased markers of apoptosis and cell-death membranes.[33] This dual effect of cell cycle arrest followed by apoptotic induction and secondary necrotic features has underscores TSA's potential as a targeted epigenetic therapy in MM.

Transcriptomic dysregulation and pathway enrichment

RNA-seq analysis following TSA exposure uncovered 1,723 DEGs, confirming the extensive transcriptional rewiring induced by HDAC inhibition. KEGG pathway enrichment revealed prominent involvement of ECM–receptor interaction, microRNA regulation, and cell-cycle pathways. The down-regulation of proliferation-associated markers such as *SPAG5*, *CCNA2,* and *MKI67* is consistent with the observed suppression of DNA replication and mitotic progression.[35,36] Conversely, the observed up-regulation of genes such as *TMEM255B*, *PCDH1,* and *METTL7A* may reflect induction of cellular stress-adaptive pathways or a shift toward more differentiated phenotypes. Notably, the increased expression of *SATB1*, a key chromatin-organising factor, suggests compensatory remodelling of nuclear architecture in response to epigenetic perturbation. For example, *METTL7A* has been shown to mediate exosome-driven chemoresistant programmes in MM.[36,37] Meanwhile, *SATB1*'s role in establishing chromatin loops and enabling rapid transcriptional reprogramming has been documented in hematopoietic progenitor contexts.[38]

Core gene clusters and survival-associated biomarkers

Our network analysis uncovered three principal functional modules in TSA-treated U266 cells: an interferon-stimulated gene cluster (*OASL*, *IFIT1*, *RSAD2*, *XAF1*), a cytoskeletal-regulator cluster (*NRCAM*, *SPTBN4*, *ANK1*), and a lipid-receptor module (*LRP1*, *APOE*, *LRP2*). These modules reflect a coordinated cellular response to HDAC inhibition, encompassing immune activation, structural remodelling, and modulation of lipid-metabolic signalling.[39] The positive survival correlation of *APOE*, *RSAD2*, *XAF1*, and *IFIT1* suggests that TSA may promote a gene-expression signature associated with improved immune recognition and reduced tumour aggressiveness. Similar findings have been reported for HDAC6 inhibitors, which enhance antigen presentation and cytotoxic T-cell responses.[11]

Biological and translational implications

The integrated cellular and transcriptomic data indicate that TSA inhibits MM progression through a dual mechanism: inducing cell-cycle arrest and modulating epigenetic programs that enhance immune activity. The upregulation of interferon-stimulated genes suggests that HDAC inhibition may increase tumor immunogenicity, which could sensitize MM cells to immunotherapies or proteasome inhibitors.[11,40] Importantly, the association of *APOE* and *RSAD2* expression with improved survival highlights their potential as survival-associated biomarkers and therapeutic targets.[41,42] The observed association of *APOE*

and *RSAD2* with improved survival in MM aligns with their roles in other age-related diseases characterized by immune dysregulation and metabolic changes. This suggests that these biomarkers may reflect underlying biological processes common to diseases of the elderly, supporting their potential as survival-associated biomarkers and therapeutic targets in MM. Overall, these findings reveal that TSA not only halts proliferation but also reprogrammes malignant plasma cells toward apoptosis and immune activation, emphasizing the translational relevance of HDAC inhibition in MM treatment.

A key limitation of this study is that the identified survival-associated biomarkers were validated only through in silico analysis of public datasets and in vitro experiments using cell lines. Validation in independent MM patient cohorts will be necessary to confirm their clinical relevance and potential prognostic utility.

CONCLUSION

TSA demonstrates potent anti-myeloma activity by simultaneously halting cell proliferation, inducing apoptosis, and reshaping the transcriptomic landscape of U266 cells. TSA-mediated enrichment of interferon signalling, extracellular matrix interactions, and lipid receptor pathways, together with the upregulation of survival-associated genes such as *APOE*, *RSAD2*, *XAF1*, and *IFIT1*, suggests a shift toward an immune-reactive, less proliferative cellular state. These findings not only reinforce the therapeutic potential of HDAC inhibition in MM but also identify molecular signatures that may serve as predictive biomarkers or targets for personalized treatment strategies, offering new avenues for improving patient outcomes. Future studies should focus on validating these biomarkers in clinical patient samples to establish their potential as survival-associated biomarkers tools.

FUNDING

This work was supported by the Universiti Sains Malaysia external agencies grant 304.PPSP.6150282.M196 from the Malaysian Society of Haematology (MSH) to M.F.J.

CONFLICT OF INTEREST

There were no conflicts of interests between the contributors of this research.

INSTITUTIONAL REVIEW BOARD (ETHICS COMMITTEE)

Ethical approval was not required for this study, as it involved only in vitro experiments using commercially available human myeloma cell lines and did not include human participants or animal subjects.

ACKNOWLEDGEMENTS

We would like to thank all the staff at the Central Research Laboratory (CRL), School of Medical Sciences, Universiti Sains Malaysia, Health Campus, for granting us permission to use the instruments and guidelines during the conduct of this study.

REFERENCES

1. Fend F, Dogan A, Cook JR. Plasma cell neoplasms and related entities-evolution in diagnosis and classification. *Virchows Arch*. Jan 2023;482(1):163-177. doi:10.1007/s00428-022-03431-3

2. Tothong W, Tantiworawit A, Norasetthada L, et al. Prevalence, Outcomes and Impact of Disease-Related Complications in the Survival of Multiple Myeloma Patients. *Hematol Rep*. Feb 21 2024;16(1):89-97. doi:10.3390/hematolrep16010009
3. Koh MY, Chung T-H, Tang NXN, et al. The ADAR1-regulated cytoplasmic dsRNA-sensing pathway is a novel mechanism of lenalidomide resistance in multiple myeloma. *Blood*. 2025;145(11):1164-1181. doi:10.1182/blood.2024024429
4. Chng W-J, Nagarajan C, Huang S-Y, et al. A systematic review on the epidemiology and treatment options of multiple Myeloma in Asia. *Heliyon*. 2024/11/15/ 2024;10(21):e39698. doi:https://doi.org/10.1016/j.heliyon.2024.e39698
5. Bishop RT, Miller AK, Froid M, et al. The bone ecosystem facilitates multiple myeloma relapse and the evolution of heterogeneous drug resistant disease. *Nature Communications*. 2024/03/19 2024;15(1):2458. doi:10.1038/s41467-024-46594-0
6. Lin CH, Tariq MJ, Ullah F, et al. Current Novel Targeted Therapeutic Strategies in Multiple Myeloma. *International Journal of Molecular Sciences*. 2024;25(11). doi:10.3390/ijms25116192
7. Kotulová J, Baďurová K, Chyra Z, et al. Novel immunotargets in multiple myeloma: biological relevance and therapeutic potential. *Biomarker Research*. 2025/07/01 2025;13(1):92. doi:10.1186/s40364-025-00799-7
8. Sutanto H, Sandra DY, Safira A, Adytia GJ, Waitupu A, Romadhon PZ. Genetic, epigenetic, and molecular determinants of multiple myeloma and precursor plasma cell disorders: a pathophysiological overview. *Med Oncol*. Jun 3 2025;42(7):234. doi:10.1007/s12032-025-02807-0
9. Ismail NH, Mussa A, Zakaria NA, et al. The Role of Epigenetics in the Development and Progression of Multiple Myeloma. *Biomedicines*. Oct 31 2022;10(11) doi:10.3390/biomedicines10112767
10. Song C, Liu X, Lin W, et al. Systematic analysis of histone acetylation regulators across human cancers. *BMC Cancer*. 2023/08/08 2023;23(1):733. doi:10.1186/s12885-023-11220-7
11. Rana PS, Ignatz-Hoover JJ, Kim BG, et al. HDAC6 Inhibition Releases HR23B to Activate Proteasomes, Expand the Tumor Immunopeptidome and Amplify T-cell Antimyeloma Activity. *Cancer Res Commun*. Jun 18 2024;4(6):1517-1532. doi:10.1158/2767-9764.Crc-23-0528
12. Pu J, Liu T, Wang X, et al. Exploring the role of histone deacetylase and histone deacetylase inhibitors in the context of multiple myeloma: mechanisms, therapeutic implications, and future perspectives. *Exp Hematol Oncol*. Apr 23 2024;13(1):45. doi:10.1186/s40164-024-00507-5
13. Mostofa A, Distler A, Meads MB, et al. Plasma cell dependence on histone/protein deacetylase 11 reveals a therapeutic target in multiple myeloma. *JCI Insight*. Dec 22 2021;6(24)doi:10.1172/jci.insight.151713
14. Harada T, Ohguchi H, Oda A, et al. Novel antimyeloma therapeutic option with inhibition of the HDAC1-IRF4 axis and PIM kinase. *Blood Adv*. Mar 28 2023;7(6):1019-1032. doi:10.1182/bloodadvances.2022007155
15. Freitas M, Issa ME, Cuendet M. Targeting the Resistance in Multiple Myeloma. *Proceedings*. 2019;11(1). doi:10.3390/proceedings2019011003
16. Elbezanti WO, Challagundla KB, Jonnalagadda SC, Budak-Alpdogan T, Pandey MK. Past, Present, and a Glance into the Future of Multiple Myeloma Treatment. *Pharmaceuticals*. 2023;16(3). doi:10.3390/ph16030415

17. Li L, Hao S, Gao M, et al. HDAC3 Inhibition Promotes Antitumor Immunity by Enhancing CXCL10-Mediated Chemotaxis and Recruiting of Immune Cells. *Cancer Immunol Res*. May 3 2023;11(5):657-673. doi:10.1158/2326-6066.Cir-22-0317
18. Parveen R, Harihar D, Chatterji BP. Recent histone deacetylase inhibitors in cancer therapy. *Cancer*. Nov 1 2023;129(21):3372-3380. doi:10.1002/cncr.34974
19. Geng Y, Liu J, Xie Y, et al. Trichostatin A promotes GLI1 degradation and P21 expression in multiple myeloma cells. *Cancer Manag Res*. 2018;10:2905-2914. doi:10.2147/cmar.S167330
20. Jasek E, Lis GJ, Jasinska M, Jurkowska H, Litwin JA. Effect of histone deacetylase inhibitors trichostatin A and valproic acid on etoposide-induced apoptosis in leukemia cells. *Anticancer Res*. Jul 2012;32(7):2791-9.
21. Hartmanis L, Ramsköld D, Hendriks GJ, et al. Deciphering direct transcriptional effects of epigenetic compounds through large-scale new RNA profiling. *Nat Commun*. Jul 18 2025;16(1):6629. doi:10.1038/s41467-025-61769-z
22. Bai M, Cui M, Li M, et al. Discovery of a novel HDACi structure that inhibits the proliferation of ovarian cancer cells in vivo and in vitro. *Int J Biol Sci*. 2021;17(13):3493-3507. doi:10.7150/ijbs.62339
23. Rafehi H, Kaspi A, Ziemann M, Okabe J, Karagiannis TC, El-Osta A. Systems approach to the pharmacological actions of HDAC inhibitors reveals EP300 activities and convergent mechanisms of regulation in diabetes. *Epigenetics*. 2017;12(11):991-1003. doi:10.1080/15592294.2017.1371892
24. Chen XT, Wu YP, Li YQ, et al. Comprehensive bioinformatics analysis reveals key hub genes linked to prognosis in multiple myeloma with drug resistance. *Medicine (Baltimore)*. Mar 7 2025;104(10):e41707. doi:10.1097/md.0000000000041707
25. Zhao S, Mo X, Wen Z, et al. Comprehensive bioinformatics analysis reveals the hub genes and pathways associated with multiple myeloma. *Hematology*. Dec 2022;27(1):280-292. doi:10.1080/16078454.2022.2040123
26. Adebayo OO, Dammer EB, Dill CD, et al. Multivariant Transcriptome Analysis Identifies Modules and Hub Genes Associated with Poor Outcomes in Newly Diagnosed Multiple Myeloma Patients. *Cancers (Basel)*. Apr 29 2022;14(9)doi:10.3390/cancers14092228
27. Hrgovic I, Doll M, Kleemann J, et al. The histone deacetylase inhibitor trichostatin a decreases lymphangiogenesis by inducing apoptosis and cell cycle arrest via p21-dependent pathways. *BMC Cancer*. Sep 30 2016;16(1):763. doi:10.1186/s12885-016-2807-y
28. Bouyahya A, El Omari N, Bakha M, et al. Pharmacological Properties of Trichostatin A, Focusing on the Anticancer Potential: A Comprehensive Review. *Pharmaceuticals (Basel)*. Oct 8 2022;15(10)doi:10.3390/ph15101235
29. Ramakrishnan VG, Miller KC, Macon EP, et al. Histone deacetylase inhibition in combination with MEK or BCL-2 inhibition in multiple myeloma. *Haematologica*. Oct 2019;104(10):2061-2074. doi:10.3324/haematol.2018.211110
30. Schneller A, Zojer N, Bolomsky A, Ludwig H. Synergistic interaction between HDAC and MCL-1 inhibitors through downregulation of BCL-XL in multiple myeloma. *Haematologica*. 09/01 2021;106(9):2516-2521. doi:10.3324/haematol.2020.277152
31. Grégoire D, Nicola G, Roberto D, Vittorio R, Régis B, Sophie B-N. Impact of XIAP protein levels on the survival of myeloma cells. *Haematologica*. 12/31 2008;94(1):87-93. doi:10.3324/haematol.13483
32. Zhou Y, Luo Q, Zeng F, et al. Trichostatin A Promotes Cytotoxicity of Cisplatin, as Evidenced by Enhanced Apoptosis/Cell Death Markers. *Molecules*. 2024;29(11). doi:10.3390/molecules29112623

33. Yang X, Cui X, Wang G, et al. HDAC inhibitor regulates the tumor immune microenvironment via pyroptosis in triple negative breast cancer. *Mol Carcinog*. Sep 2024;63(9):1800-1813. doi:10.1002/mc.23773
34. He W, Wu Y, Tang X, et al. HDAC inhibitors suppress c-Jun/Fra-1-mediated proliferation through transcriptionally downregulating MKK7 and Raf1 in neuroblastoma cells. *Oncotarget; Vol 7, No 6*. 2015;
35. Imai Y, Ohta E, Takeda S, et al. Histone deacetylase inhibitor panobinostat induces calcineurin degradation in multiple myeloma. *JCI Insight*. Apr 21 2016;1(5):e85061. doi:10.1172/jci.insight.85061
36. Qi YN, Liu Z, Hong LL, Li P, Ling ZQ. Methyltransferase-like proteins in cancer biology and potential therapeutic targeting. *J Hematol Oncol*. Aug 2 2023;16(1):89. doi:10.1186/s13045-023-01477-7
37. Wang Z, He J, Bach DH, et al. Induction of m(6)A methylation in adipocyte exosomal LncRNAs mediates myeloma drug resistance. *J Exp Clin Cancer Res*. Jan 3 2022;41(1):4. doi:10.1186/s13046-021-02209-w
38. Wilkes MC, Chae H-D, Scanlon V, et al. SATB1 Chromatin Loops Regulate Megakaryocyte/Erythroid Progenitor Expansion by Facilitating HSP70 and GATA1 Induction. *Stem Cells*. 2023;41(6):560-569. doi:10.1093/stmcls/sxad025
39. Borcoman E, Kamal M, Marret G, Dupain C, Castel-Ajgal Z, Le Tourneau C. HDAC Inhibition to Prime Immune Checkpoint Inhibitors. *Cancers*. 2022;14(1). doi:10.3390/cancers14010066
40. Shi M-Q, Xu Y, Fu X, et al. Advances in targeting histone deacetylase for treatment of solid tumors. *Journal of Hematology & Oncology*. 2024/05/31 2024;17(1):37. doi:10.1186/s13045-024-01551-8
41. Chen J, Zhu H, Chen S, Mi H. Apolipoprotein E is a Potential Biomarker for Predicting Cancer Prognosis and is Correlated with Immune Infiltration. *Onco Targets Ther*. 2024;17:199-214. doi:10.2147/ott.S447319
42. Li Y, Cui Q, Zhou B, et al. RSAD2, a pyroptosis-related gene, predicts the prognosis and immunotherapy response for colorectal cancer. *Am J Cancer Res*. 2024;14(5):2507-2522. doi:10.62347/rgjo6884